Original Article

Assessment of the sacroiliac joint in patients with axial spondyloarthritis via three-dimensional ultrashort echo time magnetic resonance imaging

Cui Ren[1#], Qiao Zhu[1#], Qing Li[2], Stefan Sommer[3,4], Xianchang Zhang[5], Huishu Yuan[1]

[1]Department of Radiology, Peking University Third Hospital, Beijing, China; [2]MR Collaborations, Siemens Healthineers Ltd., Shanghai, China; [3]Siemens Healthcare, Zurich, Switzerland; [4]Swiss Center for Musculoskeletal Imaging (SCMI), Balgrist Campus, Zurich, Switzerland; [5]MR Collaborations, Siemens Healthineers Ltd., Beijing, China

Contributions: (I) Conception and design: C Ren, Q Zhu, H Yuan; (II) Administrative support: H Yuan; (III) Provision of study materials or patients: C Ren, Q Zhu; (IV) Collection and assembly of data: C Ren, Q Zhu; (V) Data analysis and interpretation: C Ren, Q Zhu, Q Li, S Sommer, X Zhang; (VI) Manuscript writing: All authors; (VII) Final approval of manuscript: All authors.

[#]These authors contributed equally to this work.

Correspondence to: Huishu Yuan, MD. Department of Radiology, Peking University Third Hospital, 49 North Garden Road, Haidian District, Beijing 100191, China. Email: huishuy@bjmu.edu.cn.

Background: Bone erosion in the sacroiliac joint (SIJ) is highly specific for the diagnosis of axial spondyloarthritis (axSpA) and may indicate early disease progression. The 3D ultrashort echo time (3D-UTE) technique excels in providing clear contrast between the articular cartilage and the bone cortex interface. Additionally, it is emerging as a promising quantitative tool for detecting early cartilage changes. Therefore, this study aimed to evaluate the diagnostic performance of 3D-UTE sequences in identifying bone erosion in the SIJ of patients with axSpA and to clarify the potential of cartilage T2* values as a quantitative biomarker for axSpA.

Methods: This prospective study employed convenience and consecutive sampling methods to recruit patients diagnosed with axSpA in Peking University Third Hospital who met the Assessment of Spondyloarthritis International Society (ASAS) criteria and also an equal number of healthy volunteers. After providing informed consent, all participants underwent 3D-UTE sequences and conventional T2* mapping of the SIJs. Two radiologists separately interpreted the bone erosion of each SIJ on 3D-UTE sequences. Erosion detection of SIJs via computed tomography (CT) served as the standard of reference. The T2* values of the cartilage were measured and compared, and the diagnostic efficacy of the T2* value for axSpA diagnosis was evaluated.

Results: A total of 32 patients and 32 healthy volunteers were included. The 3D-UTE sequence, as separately assessed by two reviewers in terms of its ability to detect erosions, exhibited a notable level of accuracy. For the two reviewers, the respective diagnostic sensitivities were 94.7% and 92.9%, the specificities were 97.4% and 96.5%, positive predictive values were 96.7% and 95.4%, the negative predictive values were 95.9% and 94.5%, the accuracies were 96.2% and 94.9%, and the areas under the curve (AUCs) were 96.1% and 94.7%. For the detection of erosions, the interreader κ value was 0.949. The T2* values of the SIJ cartilage were significantly higher in patients with axSpA than in healthy volunteers. The intraobserver intraclass correlation coefficients (ICCs) for T2* measurements ranged between 80.5% and 82.2%. Meanwhile, the interobserver ICCs for UTE-T2* and gradient echo T2* measurements were 81.5% and 80.8%, respectively. The AUCs of the UTE-T2* values for discriminating patients with axSpA from the healthy volunteers of the two readers were 73.3% and 71.6%, respectively.

Conclusions: 3D-UTE sequences can be used as a reliable morphological imaging technique for detecting bone erosion in the SIJ. Additionally, UTE-T2* values of the cartilage may offer a quantitative method for identifying patients with axSpA.

Keywords: Axial spondyloarthritis (axSpA); sacroiliac joint (SIJ); cartilage; ultrashort echo time (UTE); T2* relaxation time

Submitted Aug 12, 2023. Accepted for publication Jan 02, 2024. Published online Feb 05, 2024.
doi: 10.21037/qims-23-1139
View this article at: https://dx.doi.org/10.21037/qims-23-1139

Introduction

Axial spondyloarthritis (axSpA) is a chronic autoimmune disorder characterized by primary axial skeletal involvement. According to the Assessment of Spondyloarthritis International Society (ASAS) criteria, active sacroiliitis is a critical imaging criterion for the diagnosis of axSpA (1). Edema of the subchondral bone marrow is an indicator of active sacroiliitis, but it may be found in patients with mechanical back pain or healthy controls (2). Structural lesions of the sacroiliac joints (SIJs), especially erosions, along with bone marrow edema (BME), improve confidence in the diagnosis of axSpA and help differentiate axSpA from other diseases (3,4). Computed tomography (CT) remains the gold standard for detecting erosions in sacroiliitis. However, ionizing radiation exposure from CT scans of the SIJs may be associated with an increased risk of pelvic malignancies, especially in young patients with suspected spondyloarthritis (SpA) (5,6).

Several studies have shown that 3D gradient echo (GRE) sequences such as volumetric interpolated breath-hold examination (VIBE) sequence and dual-echo steady-state sequence (DESS) have a higher sensitivity and accuracy than the 2D T1-weighted turbo spin echo (TSE) sequence—the most commonly used sequence—in identifying bone erosive damage in the SIJs (7-9). However, there have been few quantitative imaging studies aimed at detecting microscopic cartilage changes in the SIJ of patients with axSpA, which can occur before the appearance of cartilage morphologic defects and subchondral BME. Previous studies have shown that T2 mapping is technically feasible for quantifying the sacroiliac articular cartilage in patients with axSpA and asymptomatic controls (10,11). Both T2 mapping and T2* mapping are valuable techniques for assessing water content, collagen fiber network, and zonal variation reflecting the biochemical composition of the cartilage (12). Compared with T2 mapping, T2* mapping has a short acquisition time, primarily due to the use of a shorter echo time (TE) in the imaging sequence, which is necessary to capture the rapid decay of the transverse magnetization signal in tissues with short T2* values. Most conventional magnetic resonance imaging (MRI) sequences use a Cartesian sampling pattern, which fills k-space in a grid-like, rectilinear fashion. In contrast, the ultrashort TE (UTE) sequence uses a radial k-space sampling technique. In radial sampling, the k-space is filled using lines that radiate outward from the center to the periphery, and this provides the most crucial information for image contrast. This rapid acquisition is what makes it possible to achieve the ultrashort echo times that UTE is named for, allowing for the visualization of tissues with very short T2 relaxation times. In healthy cartilage, the tightly woven collagen network and proteoglycans restrict the motion of water molecules. This results in relatively short T2* relaxation times. Signals from the short T2* components of the articular cartilage are poorly captured by long TE sequences, which may be useful in determining early cartilage abnormalities (13,14). Although one study reported that 3D-UTE T2* mapping is feasible for SIJ cartilage imaging in asymptomatic volunteers (15), to the best of our knowledge, 3D-UTE T2* mapping in patients with axSpA has not yet been examined. Therefore, we conducted this study to assess the feasibility of the 3D-UTE sequence for detecting SIJ bone erosion in patients with axSpA using CT as a reference, to evaluate the quantitative T2* mapping from the 3D-UTE sequence in the diagnosis of axSpA, and to compare its performance with that of conventionally clinically available GRE-T2* mapping. We present this article in accordance with the STARD reporting checklist (available at https://qims.amegroups.com/article/view/10.21037/qims-23-1139/rc).

Methods

Participants

This prospective study was conducted in accordance with the Declaration of Helsinki (as revised in 2013) and was approved by the Medical Ethics Committee of Peking University Third Hospital (No. IRB00006761-M2022181). Informed consent was obtained from all the patients. This study recruited adult patients diagnosed with axSpA between July 2022 and January 2023 at Peking University Third Hospital through convenience and consecutive sampling methods. The inclusion criteria for the patients were as follow: a diagnosis of axSpA according to the 2009 ASAS classification criteria (16); without SIJ ankylosis, malignant tumors, or other SIJ lesions, except axSpA; and MRI and CT examinations completed with the interval no longer than 1 week. The same number of healthy volunteers who met the following inclusion criteria were included in the healthy control group: no inflammatory lumbosacral pain or suspicious physical examination for SpA and no traumatic joint pain. The exclusion criteria for all participants were a history of lumbosacral spine surgery, any contraindications to MRI scan (e.g., implanted metallic objects), failure to complete MR or CT examinations, and poor image quality. For healthy volunteers, only MRI scans of the SIJs were conducted due to the unavoidable ionizing radiation inherent to CT scans. To assess the disease activity of axSpA, we employed the Ankylosing Spondylitis Disease Activity Score (ASDAS) based on C-reactive protein (CRP).

Imaging protocols

Each participant was imaged using a 3T MR system (MAGNETOM Prisma, Siemens Healthineers, Erlangen, Germany). The MR protocol consisted of three conventional sequences: an oblique coronal 2D fat-suppressed (FS) T2-weighted TSE sequence, which was parallel to the long axis of the S2 vertebral body [time to repetition (TR), 3,000 ms; TE, 60 ms, field of view (FOV), 300 mm × 300 mm; slice thickness, 4 mm; resolution, 0.8×0.8×4 mm^3; readout bandwidth, 250 Hz/px; generalized autocalibrating partial parallel acquisition (GRAPPA) =2; duration, 2 min and 54 s]; an oblique 2D coronal T1-weighted TSE sequence (TR, 500 ms; TE, 9.2 ms; FOV, 300 mm × 300 mm; slice thickness, 4 mm; resolution, 0.8×0.8×4 mm^3; readout bandwidth, 224 Hz/px; GRAPPA =2; duration, 1 min and 22 s); and an axial 2D FS-T2-weighted TSE sequence (TR, 3,940 ms; TE, 58 ms; FOV, 320 mm × 320 mm; slice thickness, 4 mm; resolution, 0.8×0.8×4 mm^3; readout bandwidth, 221 Hz/px; GRAPPA =2; duration, 2 min and 49 s). The 3D-UTE sequence was used on the SIJs in the coronal oblique plane with the following scan parameters: flip angle (FA), 5°; TR, 142 ms (containing a segmented fat saturation module, with 1 fat saturation per 15 radial spokes); and total radial spokes, 49,980. The UTE data were acquired with a dual-echo acquisition scan (TEs, 0.05 and 2.5 ms) and another single-echo (TE, 5 ms) scan, in which imaging parameters were kept the same except for TEs and included the following: FOV, 300 mm × 300 mm; slice thickness, 1 mm; resolution, 1×1×1 mm^3; duration, 7 min and 57 s; and pixel bandwidth, 715 Hz. Conventional T2* mapping was also performed using a 2D-GRE sequence in a coronal oblique direction with the following parameters: number of echoes, 5; TEs, 4.58, 12.60, 20.16, 26.57, and 32.29 ms; FA, 25°; TR, 330 ms; FOV, 230 mm × 230 mm; slice thickness, 3 mm; resolution, 0.8×0.8×3 mm^3; duration, 7 min and 38 s; and pixel band bandwidths, 160, 160, 190, 260, and 260 Hz.

CT was performed on a dual-source spiral CT scanner (SOMATOM Definition Flash, Siemens Healthineers) using a tube voltage of 120 kV with variable tube current. The scan parameters were as follows: slice thickness, 4 mm; spacing, 4 mm; collimation thickness, 0.6 mm; and pixel, 512×512. In order to score erosions, oblique coronal images (with the same orientation as the above-mentioned MRI protocol) were reconstructed using the multiplane reconstruction tool with a slice thickness of 1 mm.

Image assessment

Two radiologists (Q.Z. and C.R., with 8 and 12 years of experience in radiology, respectively) interpreted the bone erosion of each SIJ on the 3D-UTE sequence in a random order. Both readers were blinded to the CT and other MR images. The same two reviewers scored the SIJ bone erosions on the CT images via consensus to generate the reference standard 1 month after all scoring on the 3D-UTE sequence was completed. The readers used all three echo images from the UTE sequence to thoroughly assess bone erosions. However, UTE-T2* mapping was exclusively used for cartilage quantification. Any disagreement regarding bone erosion was resolved through discussion with another senior radiologist until a consensus was reached. Axial images showing the full circumference of the first sacral neuroforamina were taken as an interaction

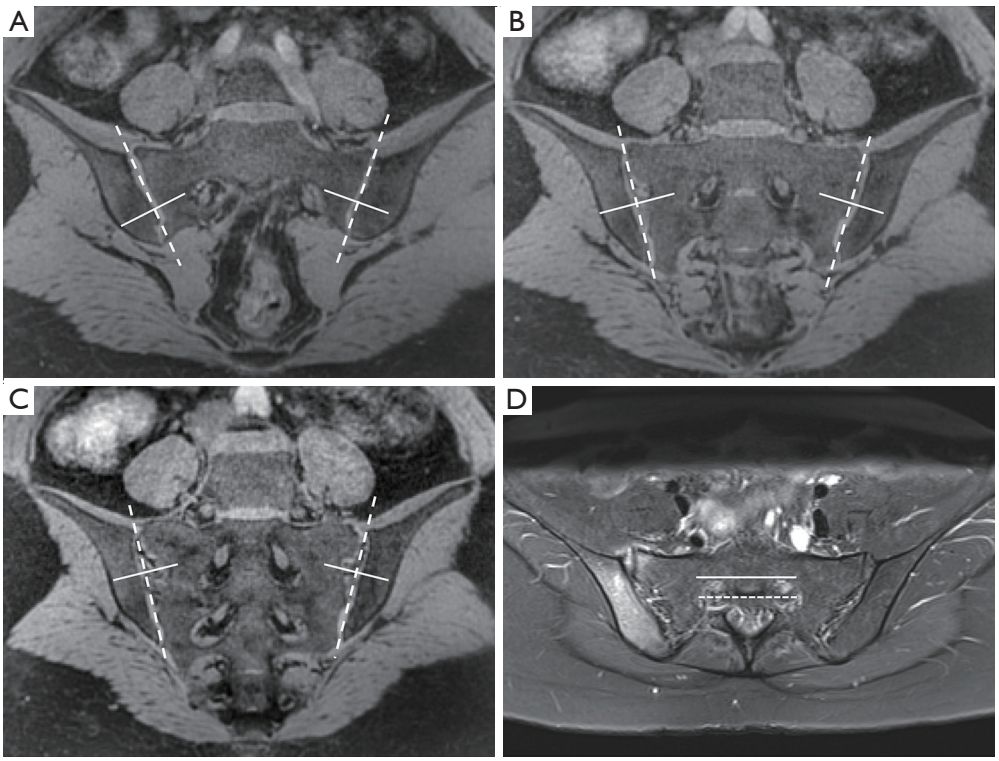

Figure 1 Oblique coronal 3D-UTE sequences at TE =0.05 ms representing the (A) anterior, (B) middle, and (C) posterior position of the sacroiliac joint. (A-C) The solid white lines are perpendicular to the joint surface (dashed white lines) across the first sacral neuroforamina that divides the sacroiliac joint into four quadrants. (D) Axial fat-saturated T2-weighted imaging showing the full circumference of the first sacral neuroforamina was used as an interaction reference to determine the directions of the sacroiliac joint. (D) The solid and dashed white lines represent the anterior and posterior wall of the first sacral neuroforamina, respectively. UTE, ultrashort TE; TE, echo time.

reference, and each SIJ on the oblique coronal images was divided into 12 subregions, including 4 quadrants (upper and lower parts of the sacral and iliac bones) and 3 directions (anterior, middle, posterior) for scoring. The upper and lower portions of the sacral and iliac bones were divided evenly by an axis perpendicular to the joint surface across the first sacral neuroforamina (9). The anterior position was defined as the slices ventral to the anterior wall of the first sacral neuroforamina. The posterior position was defined as the slices dorsal to the posterior wall of the first sacral neuroforamina and the middle position between them (*Figure 1*). Bone erosions were analyzed holistically by employing a quadrant-based approach. Presence or lack of erosions of each subregion on oblique coronal CT and 3D-UTE sequences was scored as 1 or 0, respectively. Erosion was defined as a defect in the subchondral bone associated with a full-thickness loss of the subchondral cortex at its expected location.

The UTE-T2* mapping was calculated offline using MATLAB (R2017b; MathWorks, Natick, MA, USA). For both UTE- and GRE-T2* mapping, the T2* value was fitted using the monoexponential decay model. SIJ cartilage T2* values were measured separately on 3D-UTE and GRE-T2* mapping independently by two radiologists. To assess intraobserver agreement, the same radiologist conducted a reevaluation of the T2* values with a 1-month interval between measurements. Owing to the varying layer thicknesses between the UTE-T2* and GRE-T2* mappings, the regions of interest (ROIs) for cartilage quantification were not identical across both sequences and could only be approximated. On both UTE-T2* and GRE-T2* mapping, ROIs were manually positioned within the cartilaginous part of each SIJ and were as large as possible on five consecutive central slices. Joint fluid and vacuum phenomenon (the presence of gas in the joint space) were avoided whenever possible. In addition, care was taken to avoid the cortical and subchondral bones, artifacts, and image noise. The average T2* values of the SIJs based on

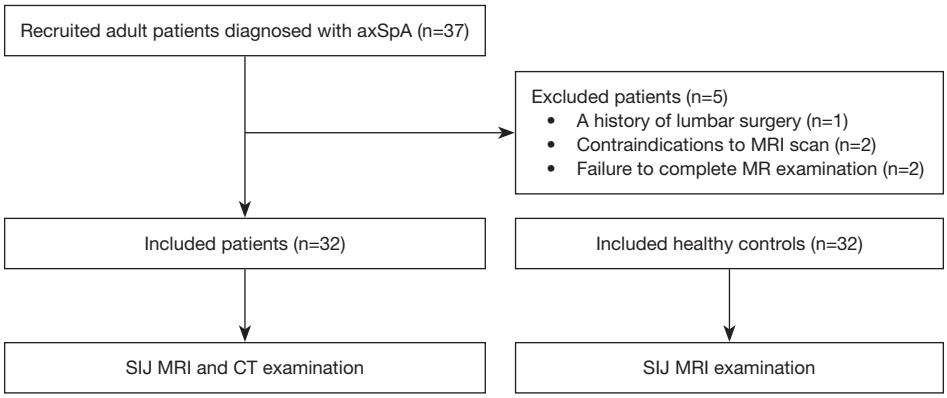

Figure 2 Flowchart of participant inclusion. axSpA, axial spondyloarthritis; MRI, magnetic resonance imaging; SIJ, sacroiliac joint; CT, computed tomography.

the 3D-UTE sequence and GRE-T2* mapping for each patient were calculated separately.

Statistical analyses

SPSS for Windows version 26.0 (IBM Corp., Armonk, NY, USA) was used for statistical analyses. All statistical analyses were performed using a two-tailed test. The Mann-Whitney test was used to compare groups for age, and a chi-squared test was used to compare the groups for sex. The sensitivity, specificity, positive predictive value, negative predictive value, and accuracy of the 3D-UTE sequence for evaluating bone erosion were calculated using CT as the reference standard. Cohen's kappa test was independently performed by two radiologists to assess the consistency of erosion on 3D-UTE sequences. To compare the difference in T2* values between the healthy and axSpA groups based on the 3D-UTE and GRE sequences, an independent-samples *t*-test was used for normally distributed data, whereas the Mann-Whitney test was used for nonnormally distributed data. We assessed the data for normality using a Q-Q plot. The intra- and interobserver agreement between the two radiologists for T2* value measurements was analyzed by calculating the interclass correlation coefficient (ICC). The ICC was evaluated as follows: 0–0.20, poor agreement; 0.21–0.40, fair agreement; 0.41–0.60, moderate agreement; 0.61–0.80, good agreement; and 0.81–1.00, excellent agreement. Receiver operating characteristic (ROC) curve analyses were performed to identify the optimal cutoff value for the diagnosis of axSpA. Specificity and sensitivity were calculated according to the cutoff value that maximized the Youden index. Areas under the curve (AUCs) were compared using MedCalc version 15.8 (Mariakerke, Belgium). A P value <0.05 indicated a statistically significant difference for all tests.

Results

Participant characteristics

The process of participant inclusion is summarized in *Figure 2*. In total, 32 patients (24 males and 8 females; mean age 28.44 years; age range, 19–67 years) with axSpA were included in this study. The duration of axSpA diagnosis ranged from 3 to 48 months, with a mean duration of 15.75 months. Among all cases, 18 had active SpA with ASDAS-CRP scores of 2.806±0.480, while 14 cases had inactive SpA with ASDAS-CRP scores of 1.107±0.114. In total, 32 healthy volunteers (19 males and 13 females; mean age 28.22 years; age range, 22–44 years) were included. There was no statistical difference between the axSpA and healthy group in terms of sex ratio (χ^2=1.772; P=0.18) or age distribution (*U*=484; P=0.71).

Diagnostic performance for bone erosion

CT detected 768 bone erosions at the quadrant level. The diagnostic performance of erosion detection on the 3D-UTE sequence is summarized in *Table 1* and *Figure 3*. For the presence or absence of erosions, the interreader agreement was excellent for the 3D-UTE sequence, and the inter-reader κ value was 0.949 (P<0.001).

Table 1 Diagnostic performance of three-dimensional ultrashort echo time sequence for bone erosion at the quadrant level with CT used as the reference

Reader	Sensitivity	Specificity	PPV	NPV	Accuracy	AUC
Reader 1	94.7% (319/337) [91.7–96.7%]	97.4% (420/431) [95.4–98.6%]	96.7% (319/330) [94.1–98.2%]	95.9% (420/438) [93.6–97.4%]	96.2% (739/768) [94.6–97.4%]	96.1% [94.4–97.7%]
Reader 2	92.9% (313/337) [89.6–95.2%]	96.5% (416/431) [94.3–97.9%]	95.4% (313/328) [92.5–97.3%]	94.5% (416/440) [92.0–96.3%]	94.9% (729/768) [93.1–96.3%]	94.7% [92.8–96.6%]

Data in parentheses are the numbers of the bone erosion subregions and data in brackets are the 95% confidence intervals. The detection success rate was determined on a per-quadrant basis: if at least one bone erosion was identifiable by the ultrashort echo time sequence, this was considered a success regardless of the total lesions identified by CT in that quadrant. CT, computed tomography; PPV, positive predictive value; NPV, negative predictive value; AUC, area under the curve.

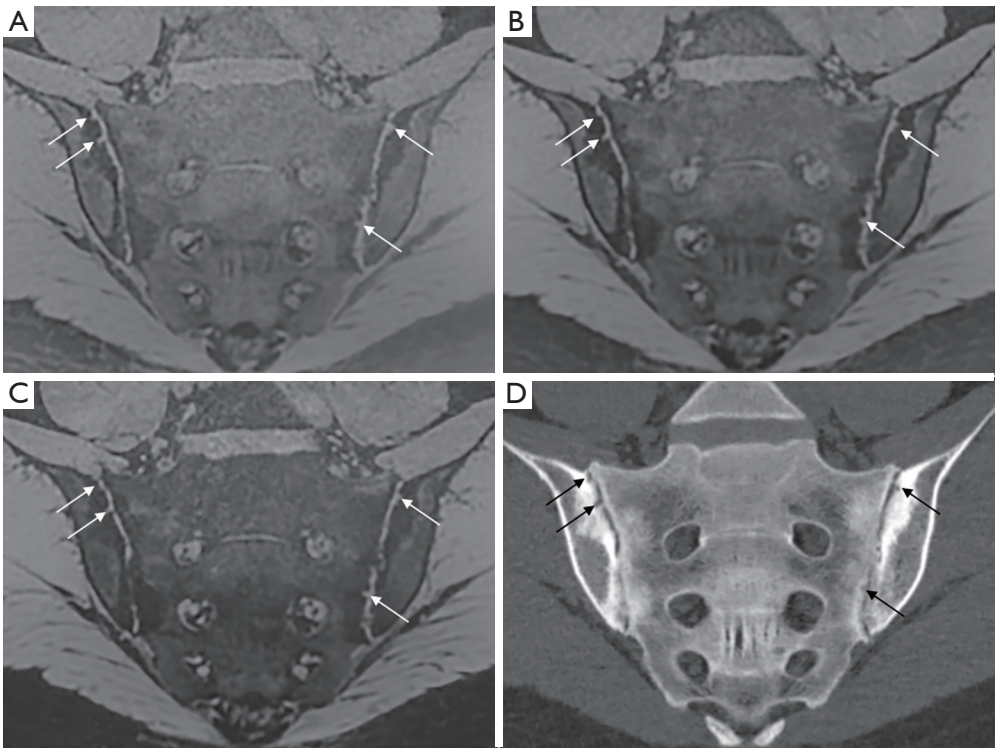

Figure 3 A 29-year-old man with axial spondyloarthritis. The oblique coronal 3D-UTE sequence at TEs of (A) 0.05 ms, (B) 2.5 ms, and (C) 5 ms revealed multiple bone erosions (solid arrows) and was consistent with (D) CT. UTE, ultrashort TE; TE, echo time.

Comparison of cartilage T2 values between the axSpA and healthy groups*

The mean T2* values of the SIJ cartilage on both 3D-UTE sequence and conventional T2* mapping measured by the two reviewers were significantly higher in those with axSpA than in healthy volunteers (P<0.05; *Table 2* and *Figures 4,5*). In addition, the T2* values of the cartilage in both patients with axSpA and healthy controls as measured by the two reviewers with the 3D-UTE sequence were higher than those measured with conventional T2* mapping (*Table 3*).

ROC curve analyses

The diagnostic efficacy of SIJ cartilage T2* measurements for axSpA identification is shown in *Table 4* and *Figure 6*. For reader 1, the AUCs for predicting axSpA using UTE-T2* and GRE-T2* values were 73.3% (95% CI: 61.0–85.6%) and 67.7% (95% CI: 54.4–80.9%), respectively; similarly,

Table 2 Comparison of T2* values of the sacroiliac joint cartilage between the axial spondyloarthritis group and the healthy group

Reader	Parameter	axSpA patients	Healthy controls	*t*	P
Reader 1	UTE-T2* (ms)	20.959±1.952	19.233±1.918	3.566	<0.001
		20.429±2.038	19.289±1.643	2.463	0.017
	GRE-T2* (ms)	19.643±1.733	18.512±1.862	2.515	0.015
		19.455±1.579	18.468±2.041	2.164	0.034
Reader 2	UTE-T2* (ms)	20.400±1.668	19.159±1.720	2.930	0.005
		20.507±1.649	19.231±2.091	2.711	0.009
	GRE-T2* (ms)	19.794±1.924	18.543±1.886	2.625	0.011
		19.873±1.778	18.886±1.549	2.366	0.021

The same radiologist obtained two measurements of the T2* values, spaced 1 month apart. Data are presented as the mean ± standard deviation. axSpA, axial spondyloarthritis; UTE-T2*, T2* values derived from UTE-T2* mapping; GRE-T2*, T2* values derived from GRE-T2* mapping; GRE, gradient echo; UTE, ultrashort echo time.

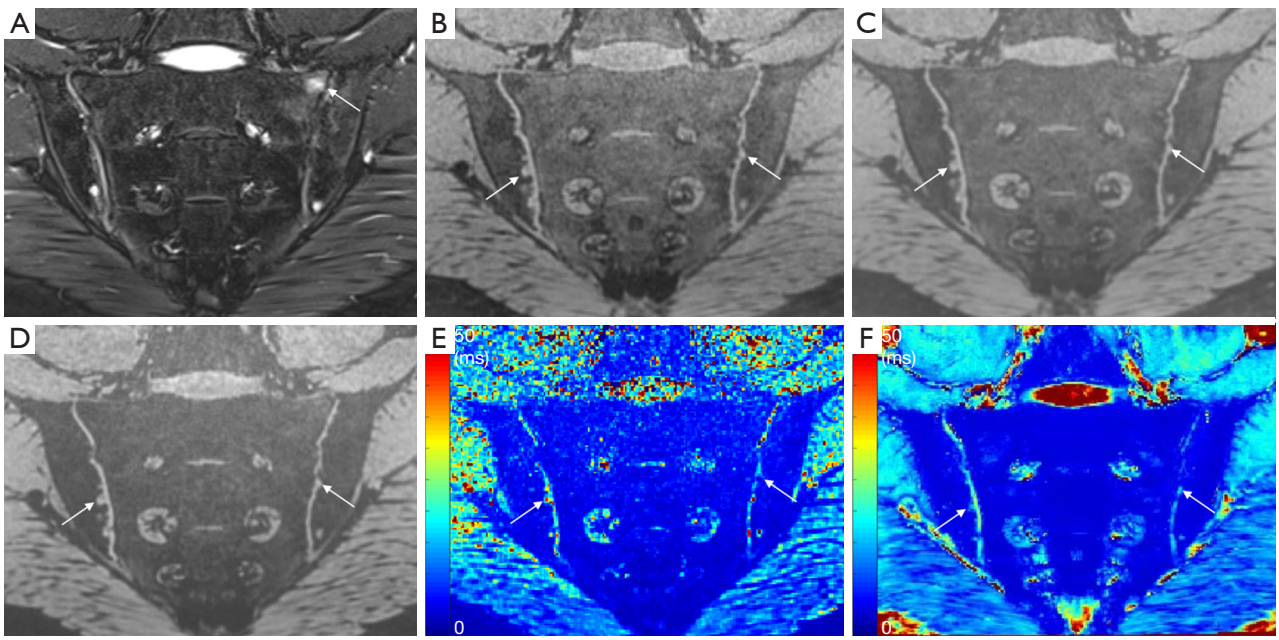

Figure 4 A 30-year-old man with axial spondyloarthritis. (A) Oblique coronal fat-saturated T2-weighted imaging of the SIJs revealed left subchondral bone marrow edema (solid arrow). The 3D-UTE sequence at TEs of (B) 0.05 ms, (C) 2.5 ms, and (D) 5 ms revealed bilateral multiple bone erosions (solid arrows). The corresponding UTE-T2* mapping (E) and conventional T2* mapping (F) revealed color-coded SIJ cartilage (solid arrows). The color gradient from green to red corresponds to the increasing T2* values of the SIJ cartilage. SIJ, sacroiliac joint; UTE, ultrashort TE; TE, echo time.

for reader 2, these AUCs were 71.6% (95% CI: 58.8–84.4%) and 67.1% (95% CI: 54.0–80.2%). The AUCs showed no significant difference between the UTE–T2* and GRE–T2* values for either reader (reader 1: Z=0.961, P=0.54; reader 2: Z=1.283, P=0.20). The T2* measurements of the SIJ cartilage showed excellent intra- and interobserver agreement (ICC 80.5–82.2%; all P values <0.001) (*Table 5*).

Discussion

The detection of structural lesions such as bone erosions plays a critical role in distinguishing axSpA from

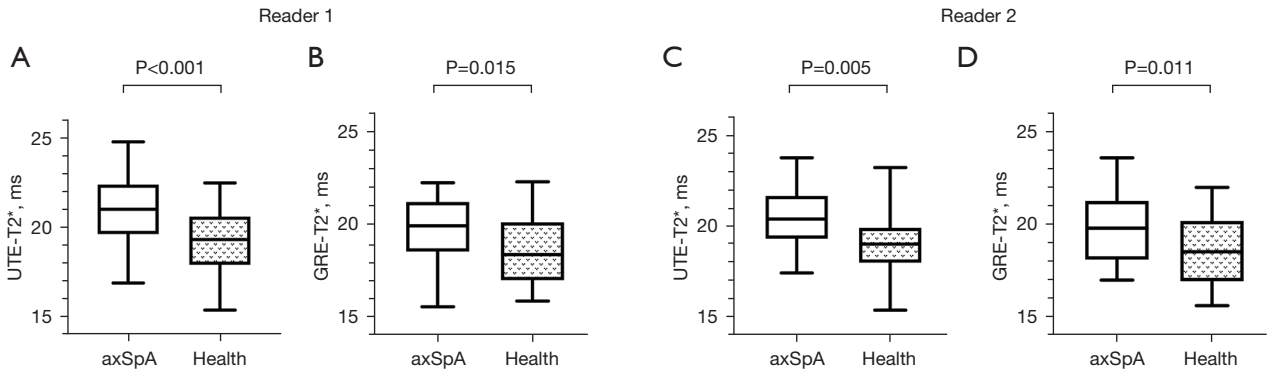

Figure 5 Box plot diagrams illustrating that the cartilage T2* values of the sacroiliac joints on both (A,C) 3D-UTE-T2* mapping and (B,D) GRE-T2* mapping are higher in patients with axSpA than in healthy controls. UTE, ultrashort echo time; GRE, gradient echo; axSpA, axial spondyloarthritis.

Table 3 Comparison of T2* values of the sacroiliac joint cartilage derived from UTE- and GRE-T2* mapping

Reader	Group	UTE-T2* (ms)	GRE-T2* (ms)	*t*	P
Reader 1	axSpA patients	20.694±1.998	19.549±1.648	3.538	<0.001
	Healthy controls	19.261±1.772	18.490±1.938	2.351	0.020
Reader 2	axSpA patients	20.454±1.646	19.833±1.838	2.011	0.046
	Healthy controls	19.195±1.900	18.715±1.721	1.498	0.137

Data are presented as mean ± standard deviation. UTE-T2*, T2* values derived from UTE-T2* mapping; GRE-T2*, T2* values derived from GRE-T2* mapping; UTE, ultrashort echo time; GRE, gradient echo; axSpA, axial spondyloarthritis.

Table 4 ROC analysis of cartilage T2* values in the diagnosis of patients with axial spondyloarthritis

Reader	Parameter	Cutoff value (ms)	Sensitivity	Specificity	AUC	95% CI	P
Reader 1	UTE-T2*	20.653	62.5%	78.1%	73.3%	61.0–85.6%	0.001
	GRE-T2*	18.420	81.3%	53.1%	67.7%	54.4–80.9%	0.015
Reader 2	UTE-T2*	18.885	84.4%	50.0%	71.6%	58.8–84.4%	0.003
	GRE-T2*	18.514	71.9%	59.4%	67.1%	54.0–80.2%	0.019

ROC, receiver operating characteristic; AUC, area under the curve; CI, confidence interval; UTE-T2*, T2* values derived from UTE-T2* mapping; GRE-T2*, T2* values derived from GRE-T2* mapping; UTE, ultrashort echo time; GRE, gradient echo.

noninflammatory mechanical conditions. A previous study using the ASAS operational definition for bone erosion reported that 90.7% of patients with SpA exhibited SIJ bone erosion, but this was observed in only 3.8% of patients with nonspecific back pain and 1.7% of healthy controls (17). In our study, the 3D-UTE sequence provided high diagnostic accuracy and interreader agreement at the quadrant level for detecting bone erosion in the SIJ. Consequently, it can be considered a valuable imaging method for the diagnosis of axSpA. The diagnostic performance of erosion detection depends on the MRI slice thickness (9,18). Chen *et al.* indicated that the thinner the slice thickness is, the higher the false-positive rate and the lower the specificity of T1-weighted imaging in diagnosing SIJ bone erosion of SpA, which may be related to the decreased signal-to-noise and contrast-to-noise ratios with a thinner slice thickness and smaller interslice gap of the 2D sequence (18). However, the 3D-UTE sequence can produce relatively thinner image slices with high in-plane resolution, which contributes to the detection of small bone erosions and an increase in

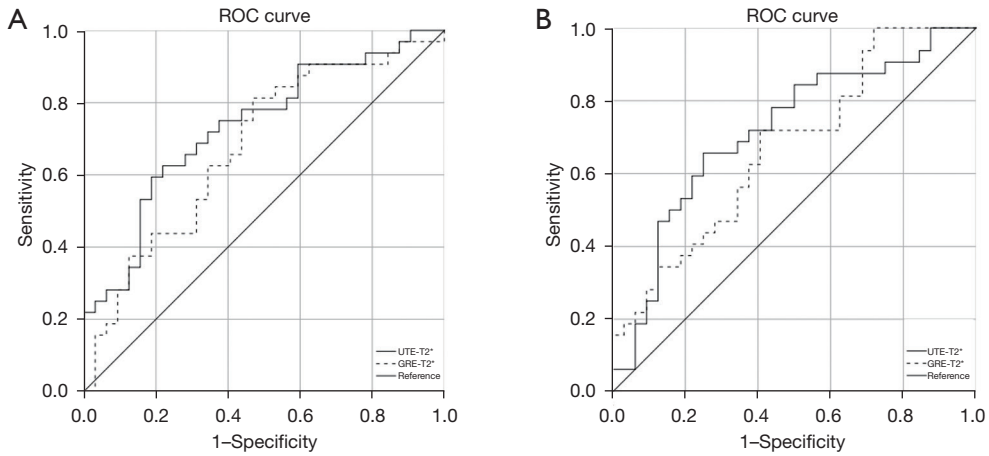

Figure 6 Receiver operating characteristic curves of ultrashort echo time and gradient echo T2* relaxation time measurements in differentiating patients with axial spondyloarthritis from healthy controls. Results from (A) reader 1 and (B) reader 2. UTE-T2*, T2* values derived from UTE-T2* mapping; GRE-T2*, T2* values derived from GRE-T2* mapping. UTE, ultrashort echo time; GRE, gradient echo; ROC, receiver operating characteristic.

Table 5 Intra- and interobserver agreement on T2* value measurement

Parameter	Reader 1		Reader 2		Interobserver	
	ICCs	95% CI	ICCs	95% CI	ICCs	95% CI
UTE-T2*	80.5%	69.9–87.7%	81.6%	71.4–88.4%	81.5%	70.9–88.4%
GRE-T2*	81.9%	71.8–88.6%	82.2%	72.3–88.8%	80.8%	70.3–87.9%

ICC, interclass correlation coefficient; CI, confidence interval; UTE-T2*, T2* values derived from UTE-T2* mapping; GRE-T2*, T2* values derived from GRE-T2* mapping; UTE, ultrashort echo time; GRE, gradient echo.

diagnostic specificity. The study by Xie *et al.* compared the VIBE sequence with different slice thicknesses and T1-weighted images for the identification of SIJ erosion detection in 96 patients suspected of SpA and found that the VIBE sequence with a 1.2-mm slice thickness was the most sensitive and accurate for erosion detection at the bone and whole-joint levels, which partially similar to our findings (9). Furthermore, cartilage, particularly at the cartilage-bone interface, comprises bound water and collagen structures with short T2* relaxation times. Although these tissues often appear dark on conventional MRI sequences due to their rapid signal decay, UTE sequences render them with a high signal. This provides outstanding contrast between the articular cartilage and the bone cortex interface. Hahn *et al.* found that 2D-UTE imaging provided better diagnostic performance for identifying SIJ bone erosion than did T1-weighted imaging and 3D DESS sequences (19). In our study, fewer erosions were detected with the 3D-UTE sequence than with CT. This observation may be attributed to the following factors: CT offers high contrast between bone and the surrounding soft tissue, which facilitates clear visualization of fine osseous details and subtle erosions. On the other hand, although MRI provides excellent soft tissue contrast, it can sometimes face limitations in spatial resolution. Consequently, some smaller erosions might not be discernible on MRI. Our research results indicated excellent consistency between the two observers when identifying bone erosion on the UTE sequence. Several factors might account for this consistency: Erosions presented with a clear and unambiguous appearance, which could have minimized ambiguity and potential variability between observers. Moreover, bone erosions were evaluated using a quadrant-based approach rather than with the one-for-one method. A comparison of the sharpness of bone erosion contours across sequences was omitted, as detection is influenced by slice thickness. In our study, the slice thickness of conventional sequences was 4 mm, while that of UTE sequences was 1 mm. The added value of

UTE sequences over conventional methods for diagnosing bone erosion warrants further exploration in subsequent research. Our results indicated that the appearance of bone erosions on UTE images was similar across different TEs. This implies that when the main objective is morphological assessment, particularly of bone erosion, an extremely short TE (e.g., 0.05 ms) in the 3D-UTE sequence may not offer significant advantages. Using a 3D-GRE sequence with a slightly longer TE may be efficient for such assessments and might reduce acquisition times and enhance resource optimization. The primary advantage of UTE sequences lies in their ability to visualize tissues with extremely short T2* relaxation times, a feature that is particularly valuable when observing the interface between articular cartilage and bone. In our subsequent study, we plan to compare the ability of the 3D-UTE sequence to diagnose SIJ bone erosion in patients with axSpA with that of the conventional 3D-GRE sequence.

To the best of our knowledge, no data are available regarding SIJ cartilage T2* measurement for axSpA assessment although UTE-T2* mapping has been widely investigated in regard to quantitatively probing articular cartilage degeneration, meniscus and ligament injuries, and enthesitis (20-23). In this study, the T2* relaxation times of the SIJ cartilage in patients with axSpA were significantly higher than those in healthy individuals in UTE-T2* mapping. Cartilage damage is a key feature of inflammatory arthritis and is caused by pannus invasion and the presence of cytokines and proteases in the synovial fluid (24). Similar to the peripheral joints, the sacroiliac cartilage is mostly composed of hyaline cartilage, with the articular surface of the ilium being a fibrocartilage that is present in childhood and converts to hyaline cartilage with age (25). As proven by CT-guided needle biopsy, cartilage abnormalities of the SIJs in axSpA manifest as degeneration, fragmentation and erosions, fibrosis, and ossification (26,27), with cartilage degeneration being the most significant manifestation of early sacroiliitis (28). Changes in early cartilage degeneration include decreased proteoglycan concentration, collagen fibril network disorganization, and increased water content in the cartilage matrix (29,30), which can lead to elevated T2* values of the cartilage. In one study, UTE-T2* imaging was able to capture signals from both long and short T2* components and was more sensitive to cartilage matrix degeneration than T2* values obtained with conventional MRI techniques (31). Previous research indicates that elevated UTE-T2* values in the knee cartilage of patients undergoing anterior cruciate ligament reconstruction can predict future osteoarthritis and correlate well with clinical biomarkers of increased osteoarthritis risk (13,32). UTE-T2* mapping can also be used to assess calcified layers of the cartilage, which may be related to the early pathogenesis of cartilage degeneration (33). Monoexponential UTE-T2* value decreases with the increasing degree of degeneration; moreover, a significant correlation between increasing short T2* fractions and worsening degrees of degeneration on bicomponent analysis has been identified (34).

One study reported that the thickness of the iliac and sacral cartilages in the SIJ ranges from 0.2 to 1.2 mm (with an average of 0.7 mm) and from 0.3 to 2.1 mm (with an average of 1.1 mm), respectively, in cadaveric specimens aged between 20 to 45 years (35). This could be one of the reasons why the calcified layers of the SIJ cartilage were not visualized in our study. As SpA frequently impacts younger individuals, we only contrasted the T2* values of the SIJ cartilage between patients with SpA and healthy volunteers. We postulate that T2* values of SIJ cartilage possess limited utility in distinguishing sacroiliitis from SIJ osteoarthritis given that the conditions may induce cartilage damage via distinct mechanisms. In our study, the eldest patient in the axSpA cohort was considerably older than the eldest volunteer. Although only one patient in each group was over 40 years old, the possibility of an age-related increase in T2* values should not be dismissed. As with other body parts, the SIJ naturally undergoes degeneration as part of the aging process. The onset of this degeneration can differ across individuals. Although the inflammation in SpA is distinct from general degeneration, prolonged inflammation may eventually result in joint degradation. Pinpointing the exact age at which SIJ degeneration commences is difficult, which is why our study did not set an age limit for the inclusion of patients with SpA. Perhaps T2* values of the SIJ cartilage could serve to differentiate patients with SpA from individuals experiencing mechanical low back pain of other origins, potentially constituting an objective of future investigations.

We found that T2* values of the SIJ cartilage derived from 3D-UTE sequence were higher than those derived from conventional T2* mapping; however, the difference was modest. Despite the two sequences being inherently different, our intention was to determine whether the UTE sequence could provide comparable, if not better, information than the conventional sequence in the context of our study. We understand that direct quantitative comparisons might be challenging, but qualitative

assessments and trend observations can still be of value. The accurate measurement of T2* relaxation times hinges on capturing the signal decay over a range of TEs. UTE sequences in our study used very short TEs (TE ≤5 ms) without including longer TE values, and they might not have optimally represented the decay curve for tissues with longer T2* values. Conversely, the GRE sequence, with a broader TE range, can capture this decay more comprehensively. Unfortunately, adding a long TE increases the TR for all acquisitions and prolongs the scan time to an impracticable total acquisition time. Fitting accuracy generally improves with a higher number of sample points (echoes). Thus, a sequence with more TEs might yield a more accurate and stable fit than would one with fewer TEs. In our study, the 3D-UTE sequence had three TEs while the conventional T2* mapping sequence had five. This difference could have influenced both the accuracy and precision of the derived T2* values. UTE sequences should ideally add voxels with shorter T2* values to the ROIs, and this addition would typically pull the mean T2* value downward. However, the mean T2* value is influenced not just by the voxels' T2* values but also by the relative contribution (or weighting) of each voxel. Other factors, such as the fitting algorithm employed and the signal-to-noise ratio, can play pivotal roles in the resultant mean value. Monoexponential fitting, which is typically used to derive T2* values, can be sensitive to noise. Indeed, we must admit that the measurement is easily affected by the surrounding structure and artifacts due to the thinness of the SIJ cartilage.

The T2* value reflects a contribution from the T2 value and additional factors related to the macromolecular content of the cartilage based on microsusceptibility effects (36). Mamisch *et al.* observed that T2* and T2 values of the knee for healthy articular cartilage and cartilage repair tissue after microfracture therapy showed a positive correlation (37). Previous studies have reported that T2 relaxation times of the SIJ cartilage were significantly higher in patients with axSpA than in healthy controls (11,38). SIJ cartilage T2* values of different anatomical regions were not compared in our study because a previous study found there to be no substantial differences across regions in healthy volunteers (15). The reproducibility of the UTE-T2* measurements of the SIJ cartilage in our study was good, although ROIs may be influenced by the partial volume effect of adjacent bone or ligamentous structures.

Our study has some limitations that should be mentioned. To begin, we used a relatively small sample size and a single-institution design. Furthermore, bone erosions were assessed holistically using a quadrant-based approach, which might have overestimated the accuracy of UTE sequences in diagnosing bone erosion. Nevertheless, our findings suggest that only minor or diminutive bone erosions could potentially elude detection on UTE sequences. When multiple bone erosions are present within a quadrant, overlooking minuscule erosions does not impede the SpA diagnosis. However, contamination of T2* relaxation measurements by joint space contents and the vacuum phenomenon cannot be ignored. Excluding the intermediate area using an automatic cartilage segmentation tool, as suggested in a prior study (10), might offer a viable solution to this issue. Additionally, longer T2* components may not be sufficiently sampled or quantified accurately with only TEs, and this may lead to inaccuracies in estimating the longer T2* values. A potential improvement for future work might include acquiring additional longer TEs to better capture and quantify the longer T2* components even if the primary interest is the shorter T2* values. Moreover, the fitting process for UTE-T2* mapping, especially with fewer TEs, might be less stable and thus more sensitive to minor fluctuations in signal intensity. This sensitivity can produce noisier maps, especially if there is a variation in the signal due to physiological factors or slight movement artifacts. Employing dual UTE sequences at varying echo times has the drawback of extending scan duration and potentially introducing motion and respiratory artifacts, which may adversely affect the precision of T2* measurements. These artifacts, chiefly concentrated in the superior region of the SIJs, were intentionally excluded during the quantification of T2* cartilage values. Despite this, our results demonstrated that the UTE-T2* measurements of the SIJ cartilage exhibited good reproducibility, implying that the influence of image artifacts was considerably mitigated. However, these problems can be reduced or even circumvented entirely through the use of a multiecho acquisition scheme, which allows for the acquisition of multiple echoes at different TEs within a single measurement. We must also consider the potential impact of both gender and age on the T2* values of SIJ cartilage. Despite there being no significant statistical difference in gender or age between our two study groups, these factors might have nonetheless influenced the results. In future research, it would be prudent to incorporate a control group that pairs each SpA patient with a healthy counterpart based on gender and age. This would help mitigate the influence of confounding variables other than SpA on the T2* values.

Finally, assessing the correlation between cartilage T2* values and histological findings can facilitate further clinical interpretation even if SIJ biopsy is not recommended in daily clinical practice.

In conclusion, our study demonstrates that 3D-UTE sequences have high diagnostic performance for SIJ bone erosion in patients with axSpA that is comparable to that of CT. Moreover, the UTE-T2* relaxation times of the SIJ cartilage may be a quantitative parameter adjunctive to standard MRI for axSpA diagnosis.

Acknowledgments

Funding: This study was supported by the grant from the Clinical Key Program of Peking University Third Hospital (No. BYSYZD2021018).

Footnote

Reporting Checklist: The authors have completed the STARD reporting checklist. Available at https://qims.amegroups.com/article/view/10.21037/qims-23-1139/rc

Conflicts of Interest: All authors have completed the ICMJE uniform disclosure form (available at https://qims.amegroups.com/article/view/10.21037/qims-23-1139/coif). Q.L. and X.Z. are employees of Siemens Healthineers Ltd. S.S. is an employee of Siemens Healthcare. The other authors have no conflicts of interest to declare.

Ethical Statement: The authors are accountable for all aspects of the work in ensuring that questions related to the accuracy or integrity of any part of the work are appropriately investigated and resolved. This study was conducted in accordance with the Declaration of Helsinki (as revised in 2013) and was approved by the Medical Ethics Committee of Peking University Third Hospital (No. IRB00006761-M2022181). Informed consent was obtained from all the patients.

References

1. Lambert RG, Bakker PA, van der Heijde D, Weber U, Rudwaleit M, Hermann KG, et al. Defining active sacroiliitis on MRI for classification of axial spondyloarthritis: update by the ASAS MRI working group. Ann Rheum Dis 2016;75:1958-63.
2. Weber U, Jurik AG, Lambert RG, Maksymowych WP. Imaging in Spondyloarthritis: Controversies in Recognition of Early Disease. Curr Rheumatol Rep 2016;18:58.
3. Seven S, Østergaard M, Morsel-Carlsen L, Sørensen IJ, Bonde B, Thamsborg G, Lykkegaard JJ, Hendricks O, Jørgensen NR, Pedersen SJ. The utility of magnetic resonance imaging lesion combinations in the sacroiliac joints for diagnosing patients with axial spondyloarthritis. A prospective study of 204 participants including post-partum women, patients with disc herniation, cleaning staff, runners and healthy persons. Rheumatology (Oxford) 2020;59:3237-49.
4. Weber U, Østergaard M, Lambert RG, Pedersen SJ, Chan SM, Zubler V, Rufibach K, Zhao Z, Maksymowych WP. Candidate lesion-based criteria for defining a positive sacroiliac joint MRI in two cohorts of patients with axial spondyloarthritis. Ann Rheum Dis 2015;74:1976-82.
5. Smith-Bindman R, Lipson J, Marcus R, Kim KP, Mahesh M, Gould R, Berrington de González A, Miglioretti DL. Radiation dose associated with common computed tomography examinations and the associated lifetime attributable risk of cancer. Arch Intern Med 2009;169:2078-86.
6. Zondervan RL, Hahn PF, Sadow CA, Liu B, Lee SI. Body CT scanning in young adults: examination indications, patient outcomes, and risk of radiation-induced cancer. Radiology 2013;267:460-9.
7. Baraliakos X, Hoffmann F, Deng X, Wang YY, Huang F, Braun J. Detection of Erosions in Sacroiliac Joints of Patients with Axial Spondyloarthritis Using the Magnetic Resonance Imaging Volumetric Interpolated Breath-hold Examination. J Rheumatol 2019;46:1445-9.
8. Algin O, Gokalp G, Ocakoglu G. Evaluation of bone cortex and cartilage of spondyloarthropathic sacroiliac joint: efficiency of different fat-saturated MRI sequences (T1-weighted, 3D-FLASH, and 3D-DESS). Acad Radiol 2010;17:1292-8.
9. Xie R, Sun D, Morelli JN, Yin C, Xiong Y, Li X.

Recognition of sacroiliac joint structural lesions: Comparison of volumetric interpolated breath-hold examination (VIBE) sequences with different slice thicknesses to T1-weighted turbo-echo. Eur J Radiol 2020;124:108849.
10. Lefebvre G, Bergère A, Rafei ME, Duhamel A, Teixeira P, Cotten A. T2 Mapping of the Sacroiliac Joints With 3-T MRI: A Preliminary Study. AJR Am J Roentgenol 2017;209:389-94.
11. Albano D, Bignone R, Chianca V, Cuocolo R, Messina C, Sconfienza LM, Ciccia F, Brunetti A, Midiri M, Galia M. T2 mapping of the sacroiliac joints in patients with axial spondyloarthritis. Eur J Radiol 2020;131:109246.
12. Guermazi A, Alizai H, Crema MD, Trattnig S, Regatte RR, Roemer FW. Compositional MRI techniques for evaluation of cartilage degeneration in osteoarthritis. Osteoarthritis Cartilage 2015;23:1639-53.
13. Williams AA, Titchenal MR, Do BH, Guha A, Chu CR. MRI UTE-T2* shows high incidence of cartilage subsurface matrix changes 2 years after ACL reconstruction. J Orthop Res 2019;37:370-7.
14. Williams A, Qian Y, Bear D, Chu CR. Assessing degeneration of human articular cartilage with ultra-short echo time (UTE) T2* mapping. Osteoarthritis Cartilage 2010;18:539-46.
15. Wong TT, Quarterman P, Duong P, Rasiej MJ, Wang R, Jaramillo D, Jambawalikar SR. A Pilot Study on Feasibility of Ultrashort Echo Time T2* Cartilage Mapping in the Sacroiliac Joints. J Comput Assist Tomogr 2021;45:717-21.
16. Rudwaleit M, van der Heijde D, Landewé R, Listing J, Akkoc N, Brandt J, et al. The development of Assessment of SpondyloArthritis international Society classification criteria for axial spondyloarthritis (part II): validation and final selection. Ann Rheum Dis 2009;68:777-83.
17. Weber U, Lambert RG, Østergaard M, Hodler J, Pedersen SJ, Maksymowych WP. The diagnostic utility of magnetic resonance imaging in spondylarthritis: an international multicenter evaluation of one hundred eighty-seven subjects. Arthritis Rheum 2010;62:3048-58.
18. Chen M, Herregods N, Jaremko JL, Carron P, Elewaut D, den Bosch FV, Jans L. Diagnostic performance for erosion detection in sacroiliac joints on MR T1-weighted images: Comparison between different slice thicknesses. Eur J Radiol 2020;133:109352.
19. Hahn S, Song JS, Choi EJ, Cha JG, Choi Y, Ju Song Y, Kim I, Park EH. Can Bone Erosion in Axial Spondyloarthropathy be Detected by Ultrashort Echo Time Imaging? A Comparison With Computed Tomography in the Sacroiliac Joint. J Magn Reson Imaging 2022;56:1580-90.
20. Afsahi AM, Sedaghat S, Moazamian D, Afsahi G, Athertya JS, Jang H, Ma YJ. Articular Cartilage Assessment Using Ultrashort Echo Time MRI: A Review. Front Endocrinol (Lausanne) 2022;13:892961.
21. Bae WC, Tadros AS, Finkenstaedt T, Du J, Statum S, Chung CB. Quantitative magnetic resonance imaging of meniscal pathology ex vivo. Skeletal Radiol 2021;50:2405-14.
22. Wilms LM, Radke KL, Latz D, Thiel TA, Frenken M, Kamp B, Filler TJ, Nagel AM, Müller-Lutz A, Abrar DB, Nebelung S. UTE-T2* versus conventional T2* mapping to assess posterior cruciate ligament ultrastructure and integrity-an in-situ study. Quant Imaging Med Surg 2022;12:4190-201.
23. Chen B, Zhao Y, Cheng X, Ma Y, Chang EY, Kavanaugh A, Liu S, Du J. Three-dimensional ultrashort echo time cones (3D UTE-Cones) magnetic resonance imaging of entheses and tendons. Magn Reson Imaging 2018;49:4-9.
24. Barendregt AM, Bray TJP, Hall-Craggs MA, Maas M. Emerging quantitative MR imaging biomarkers in inflammatory arthritides. Eur J Radiol 2019;121:108707.
25. Egund N, Jurik AG. Anatomy and histology of the sacroiliac joints. Semin Musculoskelet Radiol 2014;18:332-9.
26. Cui Y, Zhang X, Zhao Z, Liu Y, Zheng J. The relationship between histopathological and imaging features of sacroiliitis. Int J Clin Exp Med 2015;8:5904-10.
27. Egund N, Sørensen FB, Østgård R, Loft AG, Boel LWT, Jurik AG. CT-guided transarticular biopsy of the sacroiliac joint: Technique and histomorphological results. A preliminary study. Skeletal Radiol 2020;49:453-60.
28. Wang DM, Lin L, Peng JH, Gong Y, Hou ZD, Chen SB, Xiao ZY. Pannus inflammation in sacroiliitis following immune pathological injury and radiological structural damage: a study of 193 patients with spondyloarthritis. Arthritis Res Ther 2018;20:120.
29. Hesper T, Hosalkar HS, Bittersohl D, Welsch GH, Krauspe R, Zilkens C, Bittersohl B. T2* mapping for articular cartilage assessment: principles, current applications, and future prospects. Skeletal Radiol 2014;43:1429-45.
30. Choi JA, Gold GE. MR imaging of articular cartilage physiology. Magn Reson Imaging Clin N Am 2011;19:249-82.
31. Wu LL, Liu LH, Rao SX, Wu PY, Zhou JJ. Ultrashort time-to-echo T2* and T2* relaxometry for evaluation

of lumbar disc degeneration: a comparative study. BMC Musculoskelet Disord 2022;23:524.
32. Titchenal MR, Williams AA, Chehab EF, Asay JL, Dragoo JL, Gold GE, McAdams TR, Andriacchi TP, Chu CR. Cartilage Subsurface Changes to Magnetic Resonance Imaging UTE-T2* 2 Years After Anterior Cruciate Ligament Reconstruction Correlate With Walking Mechanics Associated With Knee Osteoarthritis. Am J Sports Med 2018;46:565-72.
33. de Mello R, Ma Y, Ji Y, Du J, Chang EY. Quantitative MRI Musculoskeletal Techniques: An Update. AJR Am J Roentgenol 2019;213:524-33.
34. Chang EY, Du J, Bae WC, Chung CB. Qualitative and Quantitative Ultrashort Echo Time Imaging of Musculoskeletal Tissues. Semin Musculoskelet Radiol 2015;19:375-86.
35. Puhakka KB, Melsen F, Jurik AG, Boel LW, Vesterby A, Egund N. MR imaging of the normal sacroiliac joint with correlation to histology. Skeletal Radiol 2004;33:15-28.
36. Tao H, Qiao Y, Hu Y, Xie Y, Lu R, Yan X, Chen S. Quantitative T2-Mapping and T2(*)-Mapping Evaluation of Changes in Cartilage Matrix after Acute Anterior Cruciate Ligament Rupture and the Correlation between the Results of Both Methods. Biomed Res Int 2018;2018:7985672.
37. Mamisch TC, Hughes T, Mosher TJ, Mueller C, Trattnig S, Boesch C, Welsch GH. T2 star relaxation times for assessment of articular cartilage at 3 T: a feasibility study. Skeletal Radiol 2012;41:287-92.
38. Kasar S, Ozturk M, Polat AV. Quantitative T2 mapping of the sacroiliac joint cartilage at 3T in patients with axial spondyloarthropathies. Eur Radiol 2022;32:1395-403.

Cite this article as: Ren C, Zhu Q, Li Q, Sommer S, Zhang X, Yuan H. Assessment of the sacroiliac joint in patients with axial spondyloarthritis via three-dimensional ultrashort echo time magnetic resonance imaging. Quant Imaging Med Surg 2024;14(6):4141-4154. doi: 10.21037/qims-23-1139

